HHS Public Access

Author manuscript

J Mater Chem B. Author manuscript; available in PMC 2022 September 29.

Published in final edited form as:

J Mater Chem B. ; 9(37): 7771–7781. doi:10.1039/d1tb01320c.

Injectable Silk Nanofiber Hydrogels as Stem Cell Carriers to Accelerate Wound Healing

Jiadai Li[a,b,#], **Zhaozhao Ding**[a,#], **Xin Zheng**[c], **Guozhong Lu**[d,*], **Qiang Lu**[a,*], **David L Kaplan**[e]

[a]National Engineering Laboratory for Modern Silk & Collaborative Innovation Center of Suzhou Nano Science and Technology, Soochow University, Suzhou 215123, P. R. China

[b]Nanjng University of Chinese Medicine, Nanjng 210000, P. R. China

[c]Department of Orthopedics, Taizhou Municipal Hospital, Taizhou 318000, P. R. China

[d]Engineering Research Center of the Ministry of Education for Wound Repair Technology, Jiangnan University, The Affiliated Hospital of Jiangnan University, Wuxi, 214041, P. R. China

[e]Department of Biomedical Engineering, Tufts University, Medford, Massachusetts 02155, United States

Abstract

Stem cells have potential utility in wound therapy, however the benefits are often limited due to cell injury from shear stress during injection and poor retention at the wound site. Here, shear-thinning silk nanofiber hydrogels were used to load bone marrow derived mesenchymal stem cells (BMSCs) and inject into wound sites to optimize cell retention and accelerate wound healing. The BMSCs in the silk nanofiber hydrogels maintained stemness better than the cells cultured on plates, and the expression of wound healing-related genes was significantly higher in the hydrogels with higher silk concentrations (2 wt%). The silk nanofibers physically prevented migration of BMSCs from the deposition site in the wound bed. In addition to faster wound healing, these BMSC-loaded hydrogels mediated angiogenesis and inflammation and improved collagen deposition and hair follicle regeneration *in vivo* in rats. Considering that these silk nanofiber hydrogels were successfully used here as carriers for stem cells to accelerate wound healing, further study for skin regeneration may be warranted.

Graphical Abstract

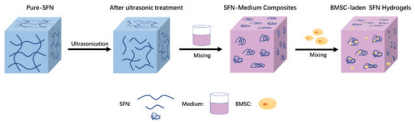

*Corresponding author: Qiang Lu, Tel: (+86)-0512-67061649, lvqiang78@suda.edu.cn, Guozhong Lu, luguozhong@hotmail.com.
#Jiadai Li and Zhaozhao Ding contributed equally to this work.

Conflict of interest

The authors declare no conflict of interest.

Injectable silk nanofiber hdyrogels were used to load stem cells and regulate cell behaviors effectively. The stem cell-laden silk hydrogels accelerated wound healing with higher quality and hair follicle regeneration.

Keywords

Silk hydrogel; Stem cells; Carriers; Wound healing; Regeneration

1. Introduction

The skin protects the body from external injury.[1,2] Multiple strategies have been pursued for skin regeneration, including grafts and dressings to promote wound healing.[3,4] However, functional recovery including the regeneration of hair follicles and sweat glands remains a challenge for full-thickness skin defects.[5, 6] Stem cells can secrete multiple factors to regulate cell behavior, such as to promote wound healing.[7, 8] Stem cells have been transplanted into wound beds to accelerate healing and functional recovery of the damaged skin.[9–11] However, these implanted stem cells migrated from the wound beds and rapidly died, thus, limiting therapeutic potential.[12] Different carriers were developed to localize and protect stem cells at wound sites to enhance efficacy towards wound healing.[13–15] However, it remains challenging to tune the cell behavior to accelerate wound regeneration, thus new biocompatible and bioactive carriers are still required to improve wound healing and functional recovery.[16]

Shear-thinning hydrogels are considered useful carriers due to their protection for stem cells during injection processes.[17] Silk fibroin (SF) has been used as a matrix in tissue regeneration because of its biocompatibility, tunable mechanical properties and degradation rate, ease of fabrication into many material formats, and limited inflammation-inducing properties.[18, 19] Recently, injectable shear-thinning SF nanofiber (SFN) hydrogels were developed, used in skin tissue regeneration and could be loaded with various bioactive molecules to tune vascularization, resulting in improved wound healing when compared to traditional silk scaffolds.[20] SFN microgels with aligned nanofiber and microporous structures were fabricated and loaded with stem cells and were dispersed into injectable SFN hydrogels, forming bioactive composite hydrogel systems to induce functional recovery in wounds.[21] These injectable SFN hydrogels exhibited tunable physical properties with different SFN concentrations, thus, we hypothesized that these injectable SFN hydrogels should provide physical cues to actively tune the paracrine activity of stem cells.[22] Thus, the goal in the present study was to load stem cells into SFN hydrogels to optimize stem cell behavior to promote wound healing, providing a simple bioactive stem cell carrier for skin regeneration, superior to previous silk-based matrices.

Here, bone marrow derived mesenchymal stem cells (BMSCs) were directly loaded in SFN hydrogels with different SFN concentrations. The loaded stem cells showed higher viability, better retention in the gels, and upregulated wound healing-related gene expression. Stem cells remained viable after injection and modulated angiogenesis and inflammation *in vivo*, promoting wound healing and improved functional recovery, including hair follicle

regeneration. The present study revealed that injectable SFN hydrogels were suitable carriers for stem cells and skin repair.

2. Materials and Methods

2.1. Preparation of Silk Nanofiber Hydrogels

Silk nanofiber hydrogels were prepared according to our previous method.[23,24] Briefly, 42.4 g Na_2CO_3 (Sinopharm Chemical Reagent Co. Ltd, China) was dissolved in distilled water (20 L) and used to degum raw silk (50 g, Zhejiang, China) at 100°C for 20 min. The degummed silk was dissolved in 9.3 mol/L LiBr (Sinopharm Chemical Reagent Co. Ltd, China) at 60°C and then dialyzed against distilled water for 3 days to remove the salt. After centrifugation at 9,000 rpm, an aqueous silk solution with a concentration of 6 wt% was obtained and further concentrated to above 20 wt% through volatilizing the solution at 60°C. The concentrated solution was diluted to 0.5 wt%, 1 wt%, 2 wt%, and 2.5 wt%, respectively, and cultured at 60°C until gel formation. All the hydrogels were composed of silk nanofibers and termed as pure-SFN0.5, pure-SFN1, pure-SFN2 and pure-SFN2.5. The samples were stored at 4°C for future use.

Ultrasonic treatment with the optimized parameters (ultrasonic power 650 W, working pulse 3 s/6 s) was used to convert pure-SFN1, pure-SFN2 and pure-SFN2.5 hydrogels into liquid solutions based on our reported process.[25] The solutions were sterilized with ^{60}Co γ-irradiation at the dose of 25 kGy. The solutions with SFN concentration of 1 wt% and 2 wt% were mixed with 2X low glucose Dulbecco's modified Eagle's medium (DMEM powder, Gibco, USA) at a ratio of 1:1, while the concentration of 2.5 wt% was mixed with 5X DMEM at a ratio of 4:1 to obtain SFN-medium blend solutions with SFN concentration of 0.5 wt%, 1 wt% and 2 wt% to facilitate the loading of BSMCs. The composite SFN carriers were termed SFN0.5, SFN1 and SFN2, respectively.

2.2. Inversion Test

Different hydrogels or solutions (2 mL) including pure-SFN0.5, pure-SFN1, pure-SFN2, SFN0.5, SFN1 and SFN2 were injected into the sample bottles and allowed to stand for 10 min before inversion to evaluate fluidity.

2.3. Injectability

The samples were added to a syringe (1 ml) and injected with or without a needle (26G) to assess injectability.

2.4. Viscoelasticity

The viscoelasticity of the samples was measured with a rheometer (AR2000, TA Instruments, USA) at room temperature. Each sample (1 ml) was added to the 20 mm cone plate (20/20) to measure the viscosity in the shear rate range from 0.1 to 100/s. The storage modulus (G') and loss modulus (G") were measured in the frequency scanning range from 1 to 100 rad/s.

2.5. AFM

The different samples were stored at 37°C for 0 and 14 days. The morphology of silk nanofibers was measured with an Atomic Force Microscope (AFM, Multimode 8, Bruker, Germany). The samples were diluted to 0.002 wt % and dropped onto fresh surfaces of mica sheets (4×4 mm^2). A 225 μm long silicon cantilever with a spring constant of 3 N m^{-1} was used in tapping mode at 0.5–1 Hz scan rate.

2.6. *In Vitro* Experiments

2.6.1. Cell Culture—Sprague-Dawley (SD) rats (40–60 g) were sacrificed to obtain BMSCs. The use of animals was in performed in compliance with the ethical requirements of experimental animals and approved by the Institutional Animal Care and Use Committee (IACUC) of Soochow University (appral number 201907A491, August 10, 2019). After the hair and muscles were removed, the femurs and tibias were cleaned with sterilized phosphate buffer saline (PBS) twice. Then the marrow cavity was cut with scissors, followed by repeat rinsing with complete medium (LG-DMEM, 10% fetal bovine serum (FBS, Gibco, USA) with 1% penicillin-streptomycin (Gibco, USA)). The cells were extracted and cultured at 37°C in a 5% CO2 incubator. Passage 3–5 BMSCs (P3-P5) were used in the experiments. BMSCs (2×10^6 cells) were added in 1 ml of SFN0.5, SFN1 and SFN2 solution. The cells were dispersed in the mixture through repeated agitation with a needle-free syringe. The cell-laden mixture (100 μL/well) was cultured in the top chamber of 24-well transwell plates (Corning Incorporated, USA) with a porosity of 0.4 microns. As a control, the same BMSCs were cultured in 6-well plates.

2.6.2. BMSC Viability—A live/dead assay was used to evaluate the viability of cells encapsulated in SFN carriers. BMSCs were stained with a LIVE/DEAD™ Viability/ Cytotoxicity Kit (Life Technologies, USA) according to the manufacturer's instructions. Calcein AM labeled live cells (green) while ethidium homodimer-1 labeled dead cells (red). The samples were imaged with confocal laser scanning microscopy (CLSM, FV10 inverted microscope, Olympus, Japan) and analyzed with ImageJ software.

2.6.3. BMSC Proliferation—The proliferation of BMSCs inside various SFN carriers was measured by deoxyribonucleic acid (DNA) content assay.[26] The cell-laden samples at the initial inoculation time were preserved and frozen at −80°C. The cell-laden samples were also cultured for 1 and 3 days, and then were refrigerated at −80°C and lyophilized with a freeze dryer (Labconco, USA). A Tissue DNA Kit (Omega, USA) was used to extract DNA according to the manufacturer's instructions. The concentrations of DNA in the samples were calculated based on a standard curve. Relative proliferation rates (RGRs) were calculated by the following formula: RGR=DNA of the cells cultured in tissue culture plates (TCP) or SFN samples /DNA of the cells at initial inoculation time ×100%.[27]

2.6.4. Migration Analysis—The 24-well transwell plates (Corning incorporated, USA) with a porosity of 8 microns were used to assess migration of BMSCs from SFN carriers. Cells were starved without serum for 12 hours before mixing. Then, 100 μL of the cell-laden mixture was placed in the top chamber while the medium containing 30% FBS as the chemotactic stimulant was added to the lower chamber. As a control, 100 μL serum-free

medium containing 2×10^4 cells was added to the upper chamber. The cells that had migrated in the lower chamber were fixed with 4% paraformaldehyde and stained with crystal violet after seeding for 24 hours. The cells were imaged with an inverted microscope (AxioVert A1, Carl Zeiss, Germany). Migration was calculated as follows: migration %=Migrated cells from SFN group/Migrated cells from the control group×100%.[28]

2.6.5 Real-Time Quantitative PCR—Real-time quantitative polymerase chain reaction (PCR) was used to measure the expression of different genes including sex determining region Y-box 2 (SOX2), octamer-binding transcription factor 4 (OCT4), angiopoietin-1 (ANGPT-1), hepatocyte growth factor (HGF), stromal cell-derived factor-1 (SDF-1) and vascular endothelial growth factor-α (VEGF-α).[29,30] After culture for 6 days, ribonucleic acid (RNA) was extracted with an RNA simple Total RNA Kit (Tiangen Biotech, China) according to the instructions. The concentration of extracted RNA was measured with a microplate reader (Synergy H1, BioTek, USA). Then, RNA was reverse transcribed to cDNA using a Prime ScriptTM RT reagent kit (Takara, Japan). Real-time qPCR was performed using SYBR Green PCR Master Mix (Applied Biosystems, USA) with an ABI 7500 RT-PCR System. The levels of beta actin were quantified in parallel as an internal control. The PCR conditions were as follows: 1 cycle of 95°C for 5 min; 40 cycles of 95°C for 10 s and 60°C for 1 min; hold at 4°C. The expression of genes of interest (Table 1) was measured using the $2^{-\Delta\Delta CT}$ method.

2.6.6. BMSC Viability After Injection—The influence of SFN carriers on the viability in the injection process was studied through evaluating cell viability after the injection with a 26 G needle. Since *in vitro* results suggested the best loading capacity with the SFN2 group, only BMSCs-laden SFN2 samples were studied in the injection process. BMSCs (2×10^6 cells/mL) were evenly dispersed in PBS or SFN2 and injected with a needle (26G) at a constant rate of 20 μL/s. BMSCs dispersed in PBS and SFN2 before injection were used as a control. Cell viability was evaluated with the live/dead assay as above.

2.7. *In vivo* Experiments

All animal experimental procedures were performed according to the guidelines for the Care and Use of Laboratory Animals of the National Institutes of Health and approved by the Institutional Animal Care and Use Committee (IACUC) of Soochow University (approval number 201909A253, September 20, 2019).

2.7.1. *In Vivo* Wound Healing Model—Thirty adult male SD rats weighing 250–300 g were used in wound healing study. Four traumas were established on each rat and treated with the following groups: the untreated control group (blank group), 200 μL SFN2-alone group without BMSCs (SFN2 group), BMSCs in 200 μL of medium group (BMSCs group), and 200 μL of SFN2 loaded with BMSCs group (SFN2+BMSCs group). After the hair was removed with an electric razor and depilatory paste, four full-thickness wounds with a diameter of 1.5 cm were generated on the back. Silicone rings (inner diameter of 1.5 cm, outer diameter of 2.5 cm) were sutured on the wound edges to prevent the wound shrinking. After the cell-laden or cell free groups were injected, all the wounds were covered with 3M films (Tegaderm, USA). Wound tissue samples were collected at day 3, 6, 10, 14, 21 and 28

after-surgery. Photos were taken to show the healing rate. The percentage of residual wound area was calculated as the unhealed wound area/original wound area×100%.

2.7.2. Bioluminescence Imaging—BMSCs were transfected with Luciferase^{+}/Green fluorescent protein^{+} virus (Luc^{+}/GFP^{+}, GENE Company, China) at a multiplicity of infection of 50 and cultured for 4 days. Then, puromycin was used to filtrate the transfected cells for the bioluminescence experiment. Six SD rats (six wounds per group) treated with BMSCs or SFN2+BMSCs were injected with 150 mg/kg D-luciferin (PerkinElmer, USA) to allow for bioluminescence. Images were obtained with an IVIS Lumina Series III (PerkinElmer, USA). The bioluminescence of each wound was subtracted from background luminescence and quantified as units of total flus using Living Image Software 4.4, PerkinElmer.

2.7.3. Histology Analysis—The samples collected from the wounds were fixed in 4% paraformaldehyde overnight and embedded in paraffin. The blocked samples were sectioned perpendicularly to the wound surface, obtaining consecutive sections with thickness of 5 μm. The sections were stained with hematoxylin eosin (H&E), Masson's trichrome, picrosirius red, mouse anti-rat CD68 (CD68, Abcam, USA), rabbit anti-rat CD206 (CD206, Abcam, USA), rabbit anti-rat CD31 (CD31, Abcam, USA) and rabbit anti-rat α-smooth muscle actin (α-SMA, Abcam, USA) according to the standard protocols.[9, 31] The sections were stained with H&E to evaluate new epidermis formation. Masson's trichrome-stained sections exhibited collagen synthesis and hair follicles while Picrosirius red-stained sections were used to calculate the ratio of collagen types III/I in the regenerated tissues. The inflammatory response at the wound sites was assessed based on the expression of the M1 macrophage marker CD68 and M2 macrophage marker CD206. Vascularization was studied by counting the blood vessels formed by CD31-positive and α-SMA-positive cells.

2.7.4. Real-Time Quantitative PCR—Tissue samples harvested on day 6 after implantation were immediately frozen in liquid nitrogen for later use. the collected tissue (100 mg) was added into a homogenate tube containing 1 ml of Trizol Reagent. Then, the tissue was ground to a liquid state and RNA was extracted with an RNA kit. The expression of ANGPT-1, HGF, SDF-1, and VEGF-α was measured using the $2^{-\Delta\Delta CT}$ method after reverse transcription and amplification steps.

2.8. Statistical analysis

All values are expressed as the mean ± SD. Statistical significance was measured using Student's unpaired t test (two-tailed). Differences among groups were detected using one-way or two-way analysis of variance (ANOVA). A p value <0.05 was considered statistically significant.

3. Results and Discussion

3.1. Performance of SFN-Medium Composites

To maintain the viability of stem cells in SFN carriers, culture medium with the required nutrients is required.[22] SFN hydrogels were prepared in a homogenous solution through

ultrasonic treatment with a silk concentration of 1 and 2 wt% (Fig. 1A). The SFN samples before and after the introduction of cell media were injectable with needles (26G) (Fig. 1B).[32] Both pure SFN and composite SFN samples exhibited typical shear-thinning behavior.[33] Viscosity increased with increasing SFN content and the pure SFN samples had lower viscosities than the SFN-medium composites with the same SFN concentrations (Fig. 1C). The modulus of SFN samples with different SFN concentrations were below 10 kPa (Fig. 1D). The increase of viscosity and modulus after the introduction of medium indicated the formation of SFN aggregates, likely due to charge interactions. AFM images revealed aggregates of 500 nm-800 nm in SFN-medium composites (Fig. 1E). The SFN aggregates remained stable without precipitation when the composites were placed at 37°C for 14 days. The results indicated that the SFN-medium composites were suitable carriers to load BSMCs and transfer the cells to the wound sites via injection.

3.2. Cell Response in SFN-Medium Composites

SFN hydrogels have been used in skin and bone regeneration.[34] BMSCs were dispersed in SFN-medium composites with different SFN concentrations and cultured for 3 days. Fluorescence microscopy revealed homogeneously dispersed cells (Fig. 2A). BMSCs encapsulated within the composites maintained more than 95% viability for at least 3 days (Fig. 2B). DNA quantification showed that relative proliferation rates (RGRs) of all three groups were above 95% at days 1 and 3 (Fig. 2C). The cells inside the different SFN-medium composites showed similar proliferation without significant differences (Fig. 2C).

Compared to culture in 2D plates, the BMSCs in 3D culture systems usually have improved stemness.[35] The secretion of two typical stemness-associated genes (Sox2 and Oct4) was measured (Fig. 2D).[36] Compared to the cells cultured on TCP, the BMSCs cultured in the SFN-medium composites exhibited significantly higher expression of Sox2 and similar expression of Oct4, to previous hydrogel systems.[21] The highest expression of Sox2 was achieved in the BMSCs in the SFN0.5 hydrogels, suggesting that stemness of BMSCs was influenced by the SFN-medium composition. Different physical/chemical cues in the SFN-medium composites could modulate the paracrine behavior of BMSCs.[37] Considering the possible application of BMSC-laden composites in skin regeneration, specific cytokines that promote wound healing, including ANGPT-1, HGF, SDF-1, and VEGF-α, were measured, and different expression levels were observed for the BMSCs among the various composites (Fig. 2E).[30, 38–40] Significantly increased secretion of ANGPT-1 and HGF and decreased expression of SDF-1 and VEGF-α were observed with the BMSCs in the different SFN-medium composites compared with those cultured on TCP. ANGPT-1 and HGF influence cell recruitment and immunomodulation and accelerate wound healing.[41,42] Although the secretion of SDF-1 and VEGF-α were inferior in the 3D culture systems, the highest expression of ANGPT-1 and HGF was observed in BMSCs cultured in SFN2, which suggested the feasibility of BMSC-laden SFN2 as wound matrices (Fig. 2E).

Cells in media can migrate rapidly from the targeted tissues after injection, decreasing the therapeutic effects of cell therapy.[43] The migration behavior of BMSCs in the composites was reduced compared with BMSCs cultured in medium alone (Fig. 3A). Higher SFN

concentration decreased cell migration. The fewest BMSCs migrated from the SFN2 group (Fig. 3B). Besides high secretion of ANGPT-1 and HGF, the suppression of cell migration in the SFN2 hydrogels further strengthened possible applications in wound healing. Therefore, BMSC-laden SFN2 hydrogels were used to study wound healing *in vivo*. Protecting cells from unwanted damage during the injection process is a significant advantage of shear-thinning hydrogels used in cell therapy.[44] Unlike cells in medium, BMSCs in SFN2 hydrogels remained viable after injection, confirming the protective function of the hydrogels against BMSC death (Fig. 3C, D).

3.3. Acceleration of Wound Healing with BMSC-laden Hydrogels

An *in vivo* migration study revealed the protective effect of SFN2 against the rapid loss of BMSCs from the deposition site. BMSCs transfected with Luc^{+}/ GFP^{+} were dispersed in cell medium and in SFN2, respectively, and injected into wounds. As expected, more than 70% of the BMSCs in the cell medium disappeared from the wound site after 3 days, and only 10% of the cells were still present after 6 days (Fig. 4B). The SFN2 stabilized the location of the BMSCs, as more than 40% of the BMSCs remained viable after 6 days in the wound sites. Even after 10 days, a few BMSCs were still viable in the wound area, suggesting the effectiveness of the SFN2 as BMSC carriers (Fig. 4A). The results showed that the delivery of BMSCs via SFN2 was superior to the local injection of BMSCs in medium, with improved cell survival and residence time at the wound sites achieved with SFN2 hydrogel carriers.

SFN hydrogels have been used to accelerate wound healing and were also endowed with vascularization capacity through the introduction of deferoxamine (DFO).[20] Recently, BMSCs were loaded onto silk hydrogel microparticles and dispersed in SFN hydrogels to achieve the functional recovery of skin where the hydrogel microparticles regulated the behaviors of BMSCs while SFN hydrogels protected the BMSCs from the damage in injection process.[21] Here, both the protection and control of BMSCs were achieved via the SFN hydrogels without the introduction of hydrogel microparticles. Compared to the complex BMSC-laden silk microparticle-SFN composite hydrogel system, similar regulation of cell paracrine signaling was achieved *in vitro* in BMSC-laden SFN carriers through tuning the concentration of SFN. BMSC-laden hydrogels with optimized SFN concentrations (2 wt%) were used to stimulate wound healing. As controls, BMSCs in medium (BMSCs group) and BMSC-free SFN hydrogels (SFN2 group) were implanted into wounds to clarify the synergistic action of SFN and BMSCs. Although the wounds did not heal completely in the blank (control) group or the SFN2 group after 21 days, faster healing was achieved for the SFN2 group, suggesting that the SFN hydrogels accelerated wound healing (Fig. 5A,B). The wounds closed completely after the introduction of BMSCs, which indicated the effective role of the implanted cells. The fastest healing occurred in the SFN2+BMSCs group, confirming the synergistic influence of SFN2 and BMSCs (Fig. 5B). The migration distance of the new epidermis after the introduction of SFN2 and BMSCs further supported this acceleration in the healing (Fig. 6A). Similar to the wound healing results, the SFN2+BMSCs group supported the most extensive re-epithelialization, superior to the SFN and BMSCs groups (Fig. 6B,i).

An *in vitro* paracrine study suggested that BMSC-laden SFN2 hydrogels stimulated the up-regulation and secretion of ANGPT1 and HGF but failed to stimulate the secretion of the VEGF-α and SDF-1 cytokines. Similar to the *in vitro* results, significantly higher expression of ANGPT1 and HGF was observed in the wounds *in vivo* when treated with BMSC-laden SFN2 hydrogels than in the control wounds (Fig. 6B, ii–v). Compared with the blank and SFN2 groups, the BMSCs and SFN2+BMSCs groups showed slightly reduced SDF-1 expression, but higher expression of VEGF-α at wound sites (Fig. 6B, ii–v). However, compared to BMSCs in medium, the expression of VEGF-α and SDF-1 was not significantly different in the wounds treated with BMSC-laden SFN hydrogels. Because of the different functions of cytokines in regulating cell behavior, *in vivo* angiogenesis and immunomodulation were investigated due to their critical roles in wound healing. Vascularization in the wound area was studied with immunohistochemistry on day 14 post-implantation, as angiogenesis is a key factor affecting the quality of wound healing.[45,46] The absence of a vascular network can lead to tissue ischemia and necrosis.[47] A gradual increase in new blood vessels appeared at the wound sites in the four groups, with the SFN2+BMSCs group fostering the most (Fig. 7A, B, C). Since both the *in vitro* and *in vivo* results indicated that the BMSC-laden SFN hydrogels had a negligible influence on the secretion of VEGF-α, the improved neovascularization in the SFN2+BMSCs group may be attributed to cell recruitment through the increased secretion of ANGPT1.

Inflammation is another important factor influencing scar formation.[48] M1 macrophages mainly kill microorganisms and play an important role in the early stages of wound repair, while M2 macrophages secrete various anti-inflammatory factors (such as interleukin-10) and extracellular matrix proteins (such as fibrin and transforming growth factor-β3) to promote cell proliferation, collagen deposition and angiogenesis.[49] The M1 (proinflammatory state)-M2 (anti-inflammatory state) switching of macrophages is a critical determinant of scarless tissue formation.[50] The up-regulation of HGF can modulate the inflammatory reaction at wound sites.[30] The number of macrophages sequentially decreased when the wounds were treated with SFN, BMSCs and BMSC-laden SFN hydrogels, respectively (Fig. 7D, E). The results suggested that the inflammatory reaction was reduced at the wound sites following the introduction of the BMSC-laden hydrogels. As expected, the highest ratio of M2/M1 macrophages was also observed in the SFN2+BMSCs group, indicating an anti-inflammatory environment for reducing scar formation (Fig. 7F).

To evaluate the quality of the regenerated skin, the deposited collagen was visualized through Masson's trichrome staining after 28 days post-implantation. The blue collagen fraction in the SFN2+BMSCs group was denser and thicker than that in the other three groups (Fig. 8A). Compared with the blank group, the other groups showed increased wound regeneration and collagen deposition. The highest collagen deposition was observed in the SFN2+BMSCs group, due to the synergistic action of the SFN and BMSCs. In addition to the best collagen deposition, the immunomodulation induced by the BMSCs-laden SFN hydrogels also reduced scar formation (Fig 8B, C, D). Besides reduced scar tissue structures (Fig 8B), the thickness of the newly formed skin in the SFN2+BMSCs group approached normal skin, confirming scarless regeneration. The ratio of type III versus type I collagen was also measured to characterize the scarless tissues in the regenerated wounds.[51] The introduction of the SFN hydrogels and BMSCs significantly increased the collagen type

III/I ratio (Fig. 8D). The synergistic action of SFN2 and BMSCs further promoted scarless tissue regeneration, with the highest collagen type III/I ratio. Similar to previous studies, the loaded BMSCs provided dynamic stimulation cues to induce skin regeneration.[6, 21] Due to the rapid migration of the implanted BMSCs from the wound sites, only a few hair follicles were regenerated in the BMSCs group, while due to the retention of BMSCs in SFN2 hydrogels, significantly more hair follicles appeared in the regenerated tissues in the SFN2+BMSCs group (Fig. 8A, E). Therefore, the SFN hydrogels with optimized SFN concentration were suitable carriers to load and transfer BMSCs. The BMSCs-laden SFN hydrogels regulated angiogenesis and inflammatory reactions actively in the wounds, resulting in faster, scarless skin regeneration with more hair follicles. Further quantified evaluations such as hydroxyproline and sulfated GAG are also valuable indicators of healing quality, which would be studied in our future study.

4. Conclusions

Shear-thinning silk nanofiber hydrogels were used to load BMSCs and regulate paracrine signaling. By tuning the concentration of the silk nanofibers, the hydrogels reduced the migration of BMSCs and promoted the secretion of various cytokines that in turn facilitated wound healing. In addition to protection of BMSCs during the injection process and BMSC retention at wound sites, the BMSC-laden hydrogels modulated angiogenesis and inflammatory reactions during wound healing, resulting in faster healing with scarless tissue formation. Silk nanofiber hydrogels with suitable cues were effective carriers for BMSCs and have potential in skin regeneration.

Acknowledgements

The authors thank the National Key R&D Program of China (2016YFE0204400) and the NIH (P41EB027062). We also thank the Social Development Program of Jiangsu Province (BE2018626) for support of this work.

References

1. Kim HS, Sun X, Lee JH, Kim HW, Fu X and Leong KW, Adv Drug Deliv Rev, 2019, 146, 209–239. [PubMed: 30605737]
2. Kurita M, Araoka T, Hishida T, O'Keefe DD, Takahashi Y, Sakamoto A, Sakurai M, Suzuki K, Wu J, Yamamoto M, Hernandez-Benitez R, Ocampo A, Reddy P, Shokhirev MN, Magistretti P, Nunez Delicado E, Eto H, Harii K and Izpisua Belmonte JC, Nature, 2018, 561, 243–247. [PubMed: 30185909]
3. Ho J, Walsh C, Yue D, Dardik A and Cheema U, Adv Wound Care (New Rochelle), 2017, 6, 191–209. [PubMed: 28616360]
4. Zeng R, Lin C, Lin Z, Chen H, Lu W, Lin C and Li H, Cell Tissue Res, 2018, 374, 217–232. [PubMed: 29637308]
5. Chouhan D, Dey N, Bhardwaj N and Mandal BB, Biomaterials, 2019, 216, 119267. [PubMed: 31247480]
6. Lim CH, Sun Q, Ratti K, Lee SH, Zheng Y, Takeo M, Lee W, Rabbani P, Plikus MV, Cain JE, Wang DH, Watkins DN, Millar S, Taketo MM, Myung P, Cotsarelis G and Ito M, Nat Commun, 2018, 9, 4903. [PubMed: 30464171]
7. Bacakova L, Zarubova J, Travnickova M, Musilkova J, Pajorova J, Slepicka P, Kasalkova NS, Svorcik V, Kolska Z, Motarjemi H and Molitor M, Biotechnol Adv, 2018, 36, 1111–1126. [PubMed: 29563048]
8. Tewary M, Shakiba N and Zandstra PW, Nat Rev Genet, 2018, 19, 595–614. [PubMed: 30089805]

9. Li T, Ma H, Ma H, Ma Z, Qiang L, Yang Z, Yang X, Zhou X, Dai K and Wang J, ACS Appl Mater Interfaces, 2019, 11, 17134–17146. [PubMed: 31008578]
10. Xuan K, Li B, Guo H, Sun W, Kou X, He X, Zhang Y, Sun J, Liu A, Liao L, Liu S, Liu W, Hu C, Shi S and Jin Y, Sci Transl Med, 2018, 10.
11. Mahmoudian-Sani MR, Rafeei F, Amini R and Saidijam M, J Cosmet Dermatol, 2018, 17, 650–659. [PubMed: 29504236]
12. Jones RE, Foster DS, Hu MS and Longaker MT, Transfusion, 2019, 59, 884–892. [PubMed: 30737822]
13. Bai T, Li J, Sinclair A, Imren S, Merriam F, Sun F, O'Kelly MB, Nourigat C, Jain P, Delrow JJ, Basom RS, Hung HC, Zhang P, Li B, Heimfeld S, Jiang S and Delaney C, Nat Med, 2019, 25, 1566–1575. [PubMed: 31591594]
14. Park S, Park HH, Sun K, Gwon Y, Seong M, Kim S, Park TE, Hyun H, Choung YH, Kim J and Jeong HE, ACS Nano, 2019, 13, 11181–11193. [PubMed: 31518110]
15. Hong KH, Kim YM and Song SC, Adv Sci (Weinh), 2019, 6, 1900597. [PubMed: 31508277]
16. Liu Z, Tang M, Zhao J, Chai R and Kang J, Adv Mater, 2018, 30, e1705388. [PubMed: 29450919]
17. Mitrousis N, Fokina A and Shoichet MS, Nature Reviews Materials, 2018, 3, 441–456.
18. Farokhi M, Mottaghitalab F, Fatahi Y, Khademhosseini A and Kaplan DL, Trends Biotechnol, 2018, 36, 907–922. [PubMed: 29764691]
19. Wang J, Chen Y, Zhou G, Chen Y, Mao C and Yang M, ACS Appl Mater Interfaces, 2019, 11, 34736–34743. [PubMed: 31518114]
20. Ding Z, Zhou M, Zhou Z, Zhang W, Jiang X, Lu X, Zuo B, Lu Q and Kaplan DL, ACS Biomater Sci Eng, 2019, 5, 4077–4088. [PubMed: 33448809]
21. Zheng X, Ding Z, Cheng W, Lu Q, Kong X, Zhou X, Lu G and Kaplan DL, Adv Healthc Mater, 2020, 9, e2000041. [PubMed: 32338466]
22. Lane SW, Williams DA and Watt FM, Nat Biotechnol, 2014, 32, 795–803. [PubMed: 25093887]
23. Bai S, Zhang X, Lu Q, Sheng W, Liu L, Dong B, Kaplan DL and Zhu H, Biomacromolecules, 2014, 15, 3044–3051. [PubMed: 25056606]
24. Zhang X, Zhang Z, Xiao L, Ding Z, He J, Lu G, Lu Q and Kaplan DL, Biomacromolecules, 2020, 21, 1022–1030. [PubMed: 31935078]
25. Bai S, Zhang X, Lu Q, Sheng W, Liu L, Dong B, Kaplan DL and Zhu H, Biomacromolecules 2014, 15, 3044–3051. [PubMed: 25056606]
26. Yuan J, Hou Q, Zhong L, Dai X, Lu Q, Li M and Fu X, Biomater Sci, 2020, 8, 5647–5655. [PubMed: 33049013]
27. Lei Z, Singh G, Min Z, Shixuan C, Xu K, Pengcheng X, Xueer W, Yinghua C, Lu Z and Lin Z, Materials Science and Engineering: C, 2018, 90, 159–167. [PubMed: 29853078]
28. Rustad KC, Wong VW, Sorkin M, Glotzbach JP, Major MR, Rajadas J, Longaker MT and Gurtner GC, Biomaterials, 2012, 33, 80–90. [PubMed: 21963148]
29. Dong Y, A S, Rodrigues M, Li X, Kwon SH, Kosaric N, Khong S, Gao Y, Wang W and Gurtner GC, Advanced Functional Materials, 2017, 27.
30. Omoto M, Suri K, Amouzegar A, Li M, Katikireddy KR, Mittal SK and Chauhan SK, Mol Ther, 2017, 25, 1881–1888. [PubMed: 28502469]
31. Wang Z, Hu W, Du Y, Xiao Y, Wang X, Zhang S, Wang J and Mao C, ACS Applied Materials & Interfaces, 2020, 12, 13622–13633. [PubMed: 32163261]
32. Amer MH, White LJ and Shakesheff KM, J Pharm Pharmacol, 2015, 67, 640–650. [PubMed: 25623928]
33. Liu Q, Zhan C, Barhoumi A, Wang W, Santamaria C, McAlvin JB and Kohane DS, Adv Mater, 2016, 28, 6680–6686. [PubMed: 27214390]
34. Kundu B, Rajkhowa R, Kundu SC and Wang X, Adv Drug Deliv Rev, 2013, 65, 457–470. [PubMed: 23137786]
35. Edmondson R, Broglie JJ, Adcock AF and Yang L, Assay Drug Dev Technol, 2014, 12, 207–218. [PubMed: 24831787]

36. Karagiannis P, Takahashi K, Saito M, Yoshida Y, Okita K, Watanabe A, Inoue H, Yamashita JK, Todani M, Nakagawa M, Osawa M, Yashiro Y, Yamanaka S and Osafune K, Physiol Rev, 2019, 99, 79–114. [PubMed: 30328784]
37. Wan S, Fu X, Ji Y, Li M, Shi X and Wang Y, Biomaterials, 2018, 171, 107–117. [PubMed: 29684675]
38. Shah AV, Birdsey GM, Peghaire C, Pitulescu ME, Dufton NP, Yang Y, Weinberg I, Osuna Almagro L, Payne L, Mason JC, Gerhardt H, Adams RH and Randi AM, Nat Commun, 2017, 8, 16002. [PubMed: 28695891]
39. Zhu Y, Hoshi R, Chen S, Yi J, Duan C, Galiano RD, Zhang HF and Ameer GA, J Control Release, 2016, 238, 114–122. [PubMed: 27473766]
40. Janela B, Patel AA, Lau MC, Goh CC, Msallam R, Kong WT, Fehlings M, Hubert S, Lum J, Simoni Y, Malleret B, Zolezzi F, Chen J, Poidinger M, Satpathy AT, Briseno C, Wohn C, Malissen B, Murphy KM, Maini AA, Vanhoutte L, Guilliams M, Vial E, Hennequin L, Newell E, Ng LG, Musette P, Yona S, Hacini-Rachinel F and Ginhoux F, Immunity, 2019, 50, 1069–1083 e1068. [PubMed: 30926233]
41. Staton CA, Valluru M, Hoh L, Reed MWand Brown NJ, Br J Dermatol, 2010, 163, 920–927. [PubMed: 20633009]
42. Jinnin M, Ihn H, Mimura Y, Asano Y, Yamane K and Tamaki K, Nucleic Acids Res, 2005, 33, 3540–3549. [PubMed: 15972796]
43. Nishiwaki K, Aoki S, Kinoshita M, Kiyosawa T, Suematsu Y, Takeoka S and Fujie T, J Biomed Mater Res B Appl Biomater, 2019, 107, 1363–1371. [PubMed: 30265776]
44. Roche ET, Hastings CL, Lewin SA, Shvartsman D, Brudno Y, Vasilyev NV, O'Brien FJ, Walsh CJ, Duffy GP and Mooney DJ, Biomaterials, 2014, 35, 6850–6858. [PubMed: 24862441]
45. Wang M, Wang C, Chen M, Xi Y, Cheng W, Mao C, Xu T, Zhang X, Lin C, Gao W, Guo Y and Lei B, ACS Nano, 2019, 13, 10279–10293. [PubMed: 31483606]
46. Veith AP, Henderson K, Spencer A, Sligar AD and Baker AB, Adv Drug Deliv Rev, 2019, 146, 97–125. [PubMed: 30267742]
47. Kameyama H, Udagawa O, Hoshi T, Toukairin Y, Arai T and Nogami M, Leg Med (Tokyo), 2015, 17, 255–260. [PubMed: 25794881]
48. Coentro JQ, Pugliese E, Hanley G, Raghunath M and Zeugolis DI, Adv Drug Deliv Rev, 2019, 146, 37–59. [PubMed: 30172924]
49. Kong X, Fu J, Shao K, Wang L, Lan X and Shi J, Acta Biomater, 2019, 100, 255–269. [PubMed: 31606531]
50. Kim H, Wang SY, Kwak G, Yang Y, Kwon IC and Kim SH, Adv Sci (Weinh), 2019, 6, 1900513. [PubMed: 31637157]
51. Kathju S, Gallo PH and Satish L, Birth Defects Res C Embryo Today, 2012, 96, 223–236. [PubMed: 23109318]

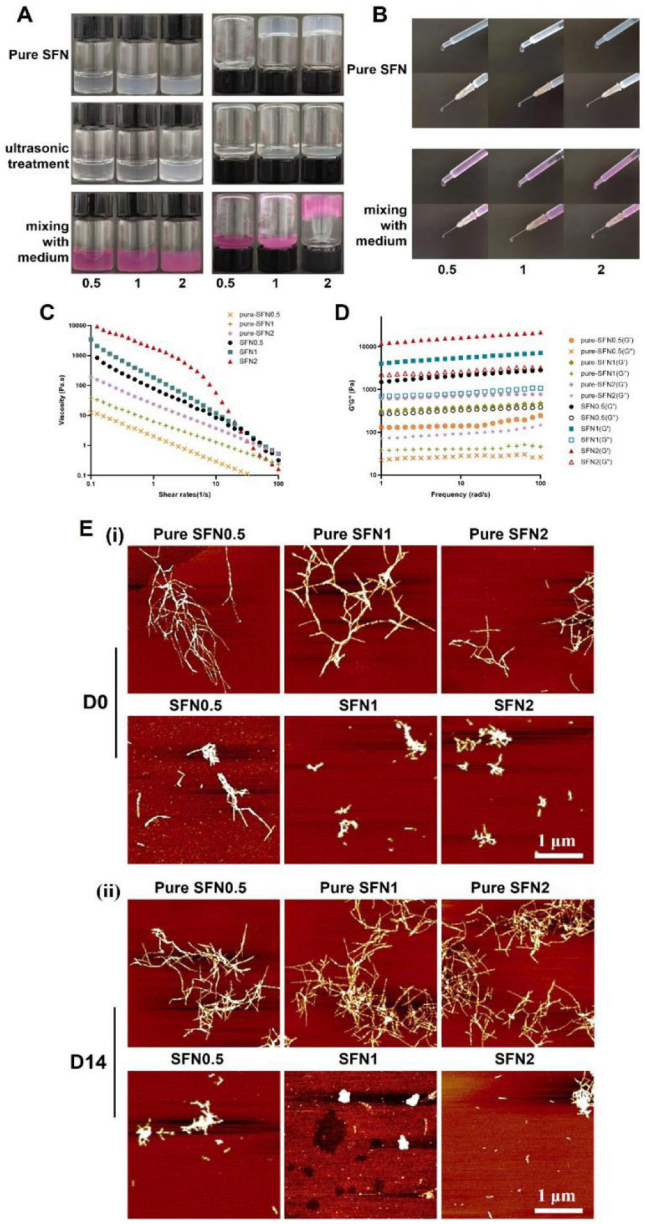

Figure 1.

Characterization of the SFN samples before and after the introduction of cell media: (A) Inversion test for 10 min; (B) Injection results. Pure means medium-free SFN samples. 0.5, 1 and 2 indicate SFN concentrations; (C) Viscosity of different samples at 25°C; (D) Storage modulus (G') and loss modulus (G") of different samples at 25°C; (E) AFM images of SFN in the samples when placed at 37°C for 0 and 14 days. Scale bars=1 μm.

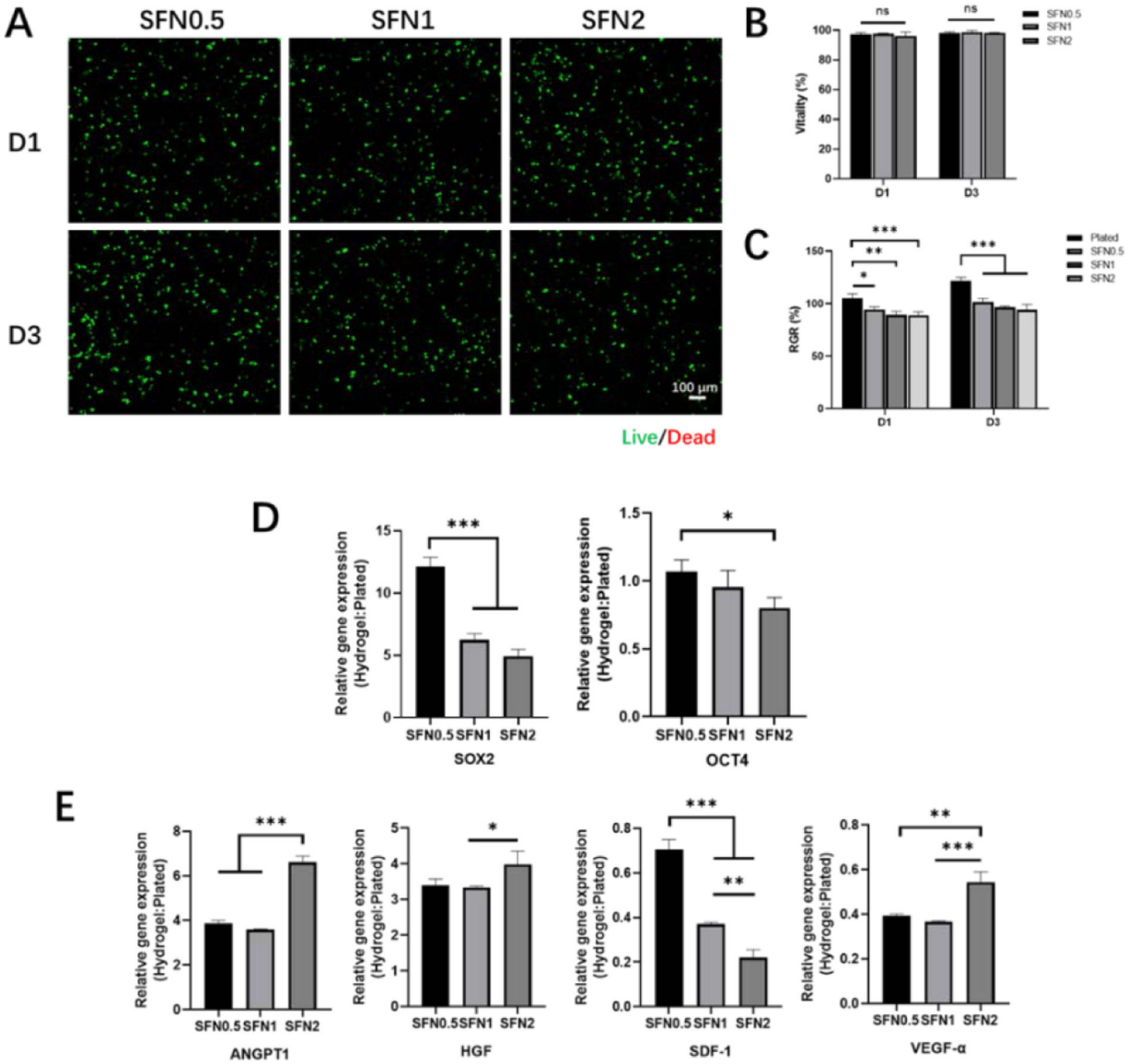

Figure 2.

Biocompatibility and gene expression of BMSCs in SFN-medium composites: (A) CLSM images of BMSC-laden composites when cultured for 1 and 3 days. Live (green) cells are labeled with Calcein AM and dead (red) cells labeled with ethidium homodimer-1. Scale bars 100 μm. (B) Viability of BMSCs encapsulated within composites on days 1 and 3; (C) Relative proliferation rates of BMSCs on days 1 and 3. (D) Relative expression of stemness genes for BMSCs cultured in different composites on day 6. Cells cultured on plates as controls. (E) Relative expression of wound healing-associated cytokine genes for BMSCs cultured in the composites on day 6. Cells cultured on plates as controls. Data presented as mean ± SD, n=3. Statistically significant *$p < 0.05$, **$p < 0.01$, and ***$p < 0.001$.

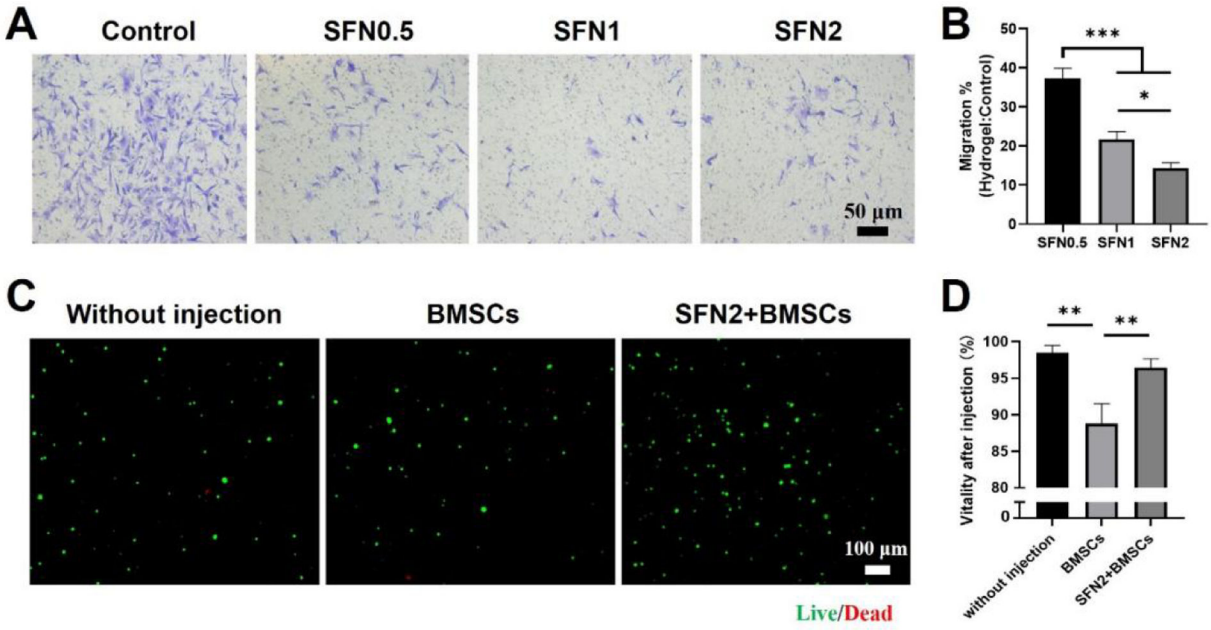

Figure 3.

Cell migration in SFN-medium composites and viability after injection: (A) Images of migrated cells after 24 hours, stained (light purple) with crystal violet. (B) Relative migration rates of BMSCs from the SFN-medium composites compared to culture medium control group. (C) CLSM images of BMSCs before and after injection with a 26 G needle. Live (green) cells labeled with Calcein AM and dead (red) cells labeled with ethidium homodimer-1. BMSC group means BMSCs cultured in medium and injected from the needle while SFN2+BMSC group indicates BMSCs loaded in SFN2 and injected from the needle. (D) Cell viability after injection. Data presented as mean ± SD, n=3. Statistically significant *$p < 0.05$, **$p < 0.01$, and ***$p < 0.001$.

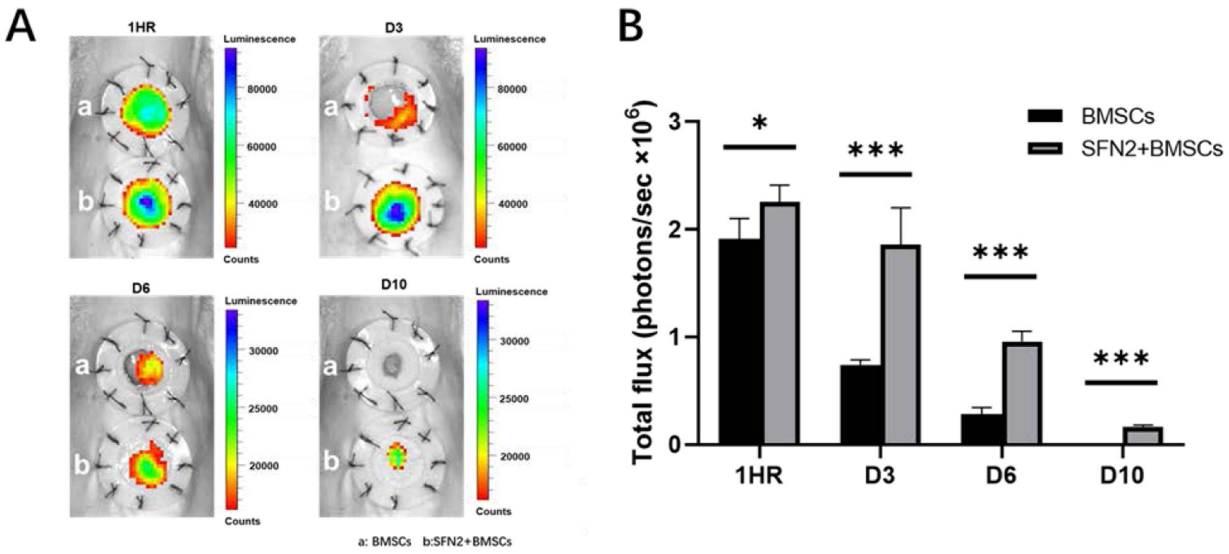

Figure 4.

In vivo retention of BMSCs loaded in SFN hydrogel system. (A) Bioluminescence imaging of Luc^{+}/GFP^{+} BMSCs in the wound area at different times. The inner diameter of silicone splints was 1.5 cm. (B) Quantification of total flux between BMSCs in medium (BMSCs) and BMSCs loaded in SFN2 hydrogels (SFN2+BMSCs). Data presented as mean ± SD, n=6. Statistically significant *$p < 0.05$, **$p < 0.01$, and ***$p < 0.001$.

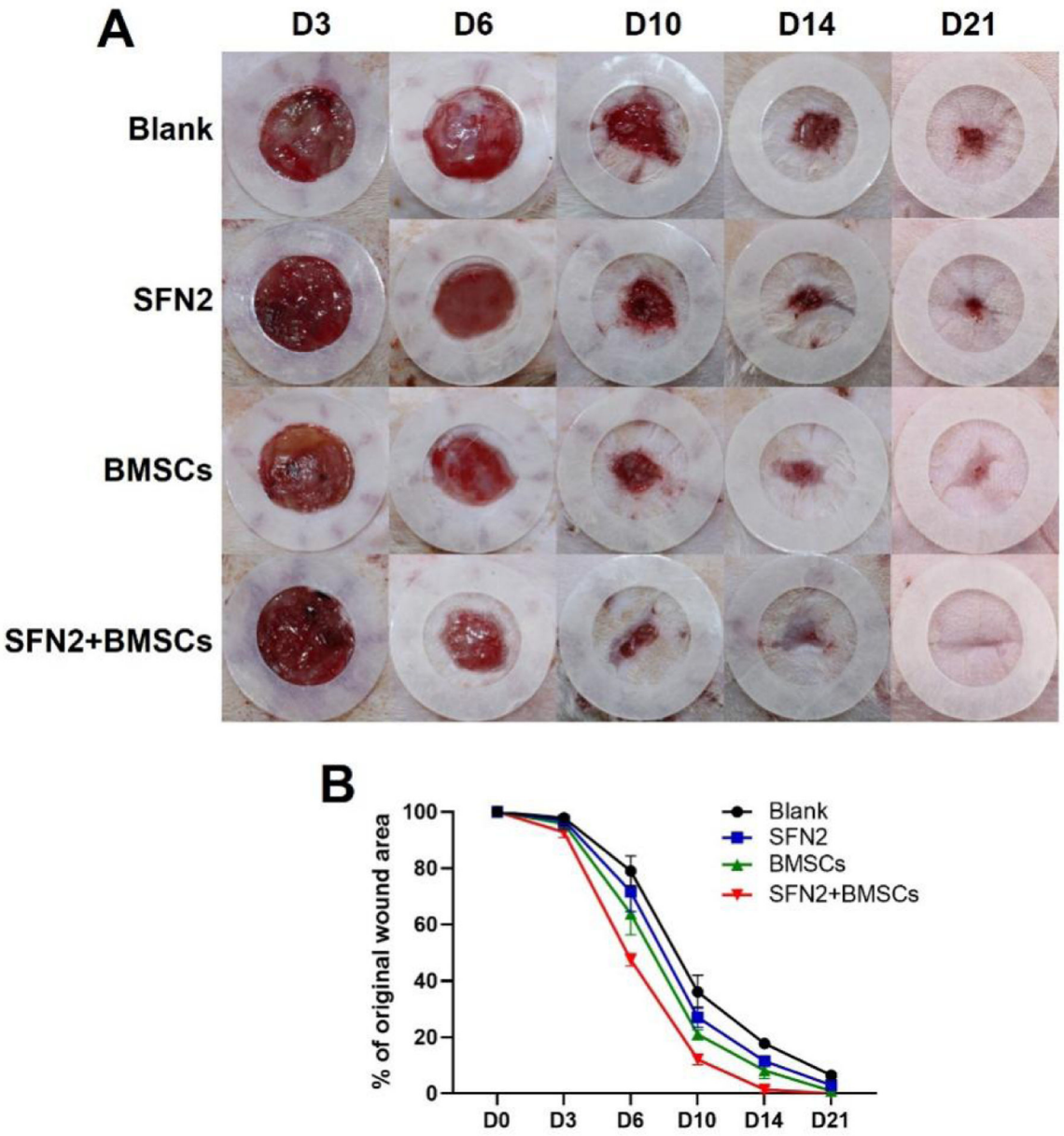

Figure 5.

Wound healing: (A) Photos of wounds treated with the different groups at days 3, 6, 10, 14 and 21 post-implantation. The inner diameter of the silicone splints was 1.5 cm; (B) Wound closure curves when treated with the various groups.

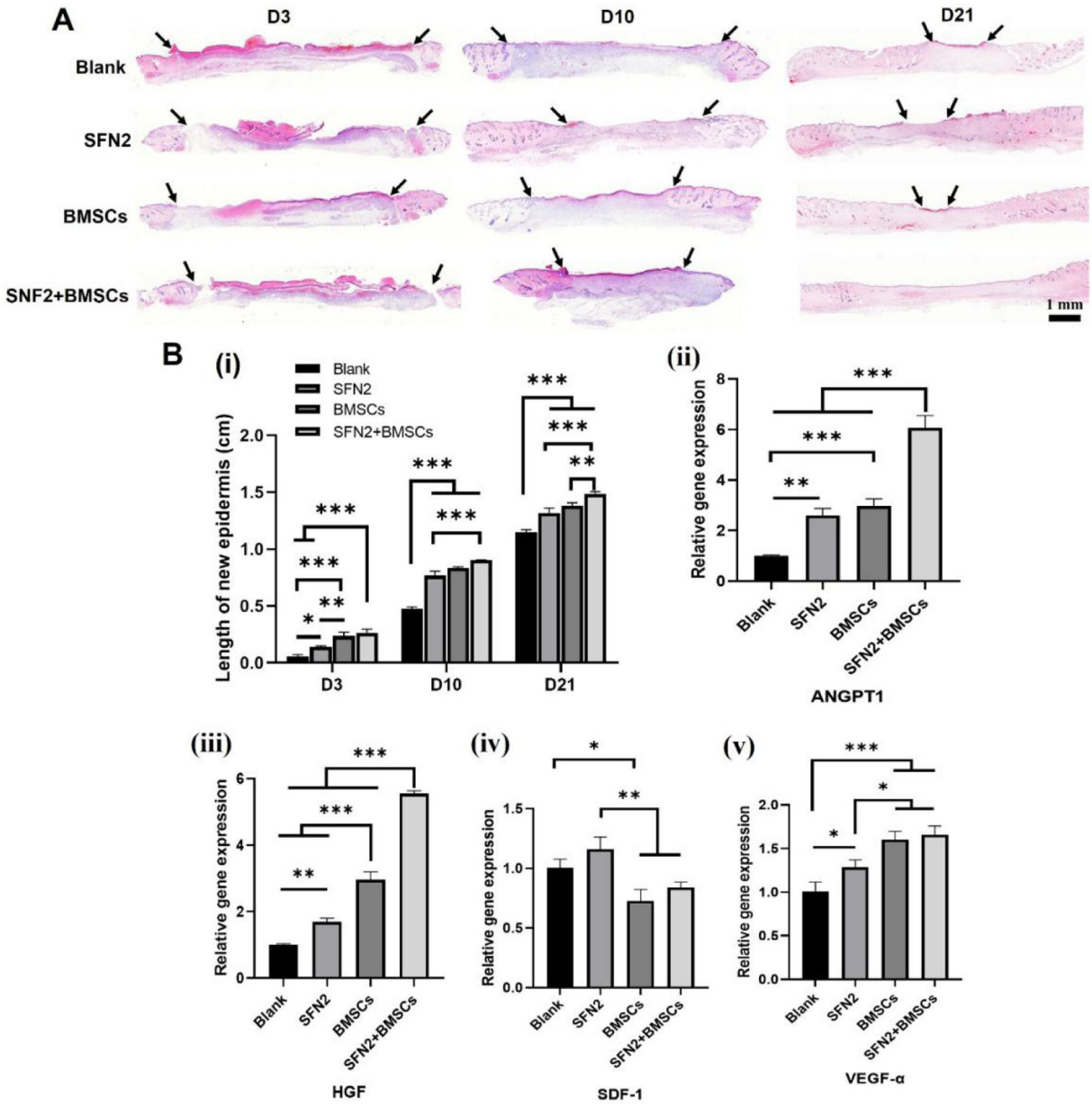

Figure 6.

Wound regeneration: (A) Hematoxylin and eosin (H&E) images of wounds treated with the different groups for 3, 10, and 21 days. Scale bars 1 mm. Arrow indicates the epithelial junction; (B,i) The length of new epidermis at days 3, 10 and 21 post-implantation; (B, ii-v) Wound healing-associated cytokine gene expression at wound sites on day 6 post-implantation. Data presented as mean ± SD, n=3. Statistically significant *$p < 0.05$, **$p < 0.01$, and ***$p < 0.001$.

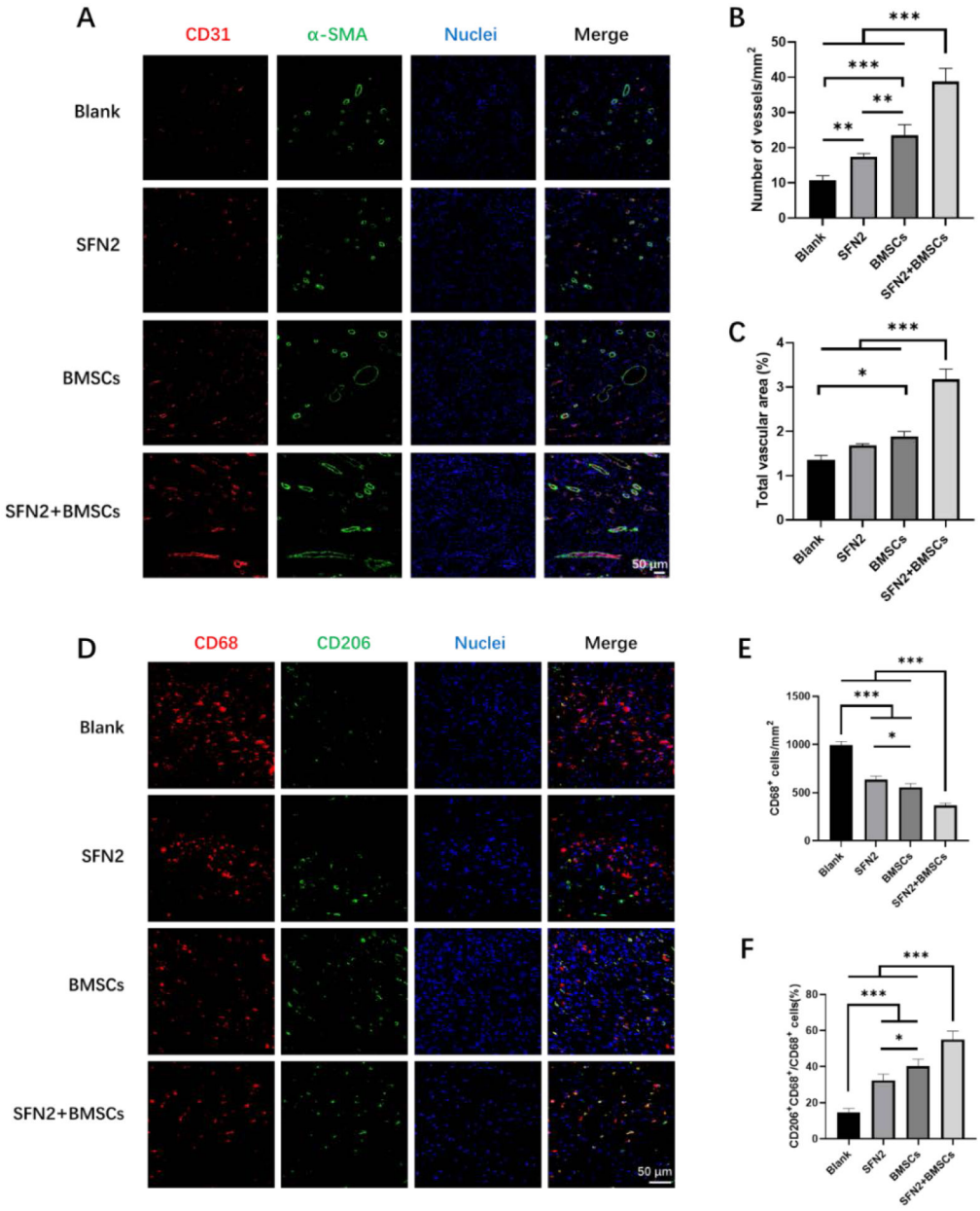

Figure 7.

Angiogenesis and immunoregulation at wound sites in the different groups after 14 days post-surgery. (A) Immunofluorescent images of tissue sections stained with CD31 antibody (red), α-SMA antibody (green) and DAPI (blue). Scale bars 50 μm. (B) Blood vessel numbers per mm^2 at wound sites treated with the different groups. (C) Percentage of CD31 vessel volume in fluorescent images. (D) Immunofluorescent images of tissue sections stained with CD68 antibody (red), CD206 antibody (green) and DAPI (blue). Scale bars 50 μm. (E) $CD68^+$ macrophage number per mm^2 at wound sites treated with the different groups. (F) Percentage of M2 macrophages over total $CD68^+$ macrophages at wound sites treated with different treatment groups. Data presented as mean ± SD, n=5. Statistically significant *$p < 0.05$, **$p < 0.01$, and ***$p < 0.001$.

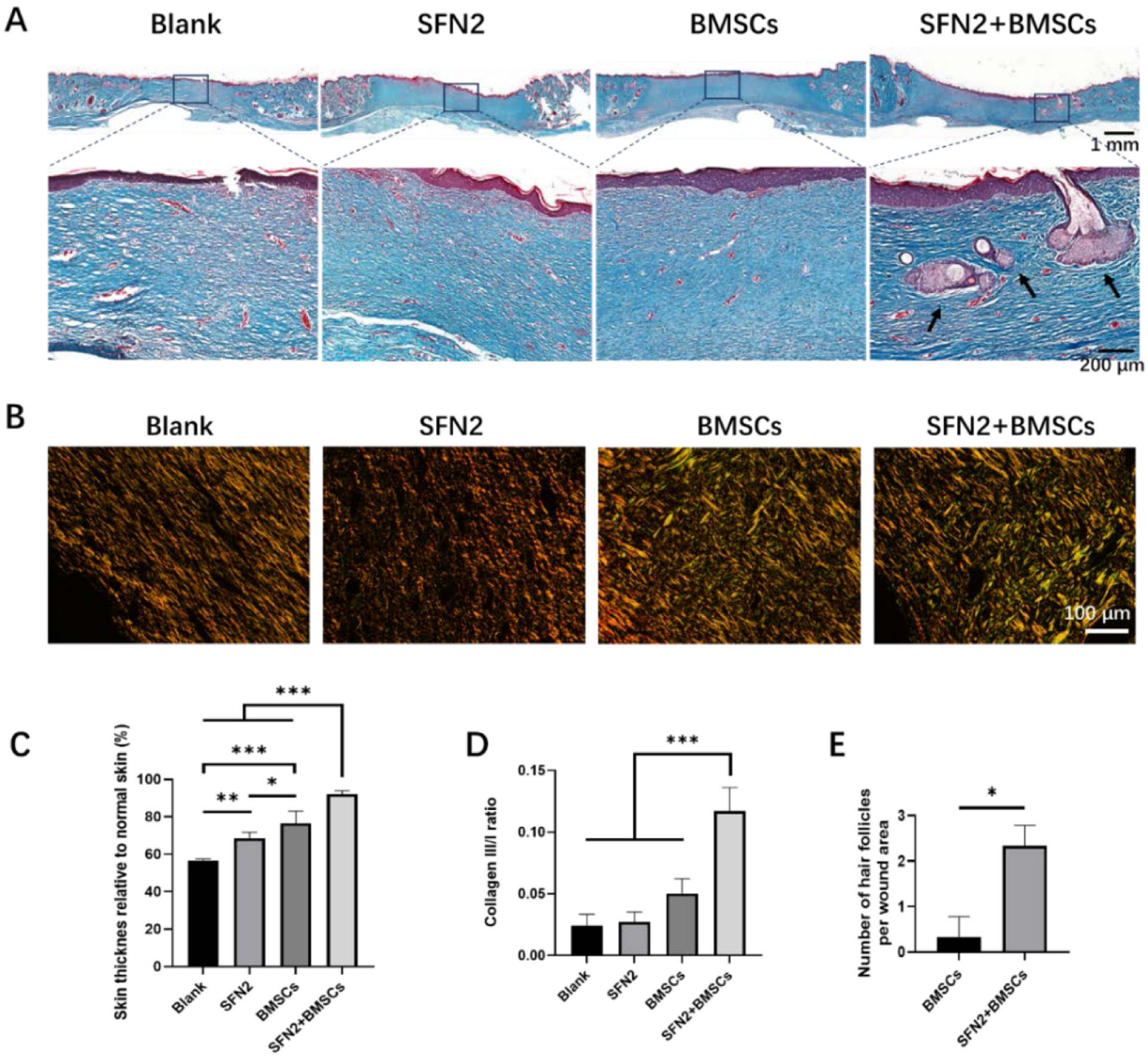

Figure 8.

Wound healing assessment after 28 days. (A) Masson's trichrome staining of regenerated tissues in the different groups. Scale bars 200 μm. (B): Picrosirius red staining of the regenerated tissues. Type I collagen in the images shown orange or yellow fibers while type III collagen shown as green fibers. Scale bars 100 μm. (C) Skin thickness in the different groups. (D)m Collagen type III/I ratio. (E) Number of hair follicles in wound area. Data presented as mean ± SD, n=3. Statistically significant *p < 0.05, **p < 0.01, and ***p < 0.001.

Table 1.

Sequences of primers used for qPCR analysis of BMSC gene expression.

Name	
GAPDH	F: 5’ TGGGTGTGAACCACGAGAA3’
	R: 5’ GGCATGGACTGTGGTCATGA3’
SOX2	F: 5’ GCCGAGTGGAAACTTTTGTCG3’
	R: 5’ CGGGAAGCGTGTACTTATCCTT3’
OCT4	F: 5’ GTGTTCAGCCAGACAACCATCT3’
	R: 5’ GGTCTCCGATTTGCATATCTCCT3’
ANGPT1	F: 5’ AGTCGGAGATGGCCCAGATA3’
	R: 5’ TGGATTTCAAGACGGGATGTT3’
HGF	F: 5’ AACAAGGGCTTTCCATTCACT3’
	R: 5’ TGTCCCCTTATAGCTGCCTCC3’
SDF-1	F: 5’ TGCATCAGTGACGGTAAGCCA3’
	R: 5’ CTTTTCAGCCTTGCAACAATC3’
VEGF-α	F: 5’ GCCCTGAGTCAAGAGGACAG3’
	R: 5’ GAGGAGGAGGAGCCATTACC3’